Letter
Vol. 46, No. 9 / 1 May 2021 / Optics Letters 2147
Optics Letters

2 Gbps free-space ultraviolet-C communication based on a high-bandwidth micro-LED achieved with pre-equalization

Shijie Zhu,[1,†] Pengjiang Qiu,[1,†] Zeyuan Qian,[1] Xinyi Shan,[1] Zhou Wang,[1] Ke Jiang,[2,3] Xiaojuan Sun,[2,3] Xugao Cui,[1] Guoqi Zhang,[1] Dabing Li,[2,3,4] and Pengfei Tian[1,*]

[1]Institute for Electric Light Sources, School of Information Science and Technology, and Academy of Engineering and Technology, Fudan University, Shanghai, 200433, China
[2]State Key Laboratory of Luminescence and Applications, Changchun Institute of Optics, Fine Mechanics and Physics, Chinese Academy of Sciences, Changchun 130033, China
[3]Center of Materials Science and Optoelectronics Engineering, University of Chinese Academy of Sciences, Yuquan Road No. 19, Beijing 100049, China
[4]e-mail: lidb@ciomp.ac.cn
*Corresponding author: pftian@fudan.edu.cn

Received 24 February 2021; revised 2 April 2021; accepted 3 April 2021; posted 5 April 2021 (Doc. ID 423311); published 26 April 2021

In this Letter, we experimentally achieve high-speed ultraviolet-C (UVC) communication based on a 276.8 nm UVC micro-LED. A record −3 dB optical bandwidth of 452.53 MHz and light output power of 0.854 mW at a current density of 400 A/cm^2 are obtained with a chip size of 100 μm. A UVC link over 0.5 m with a data rate of 2 Gbps is achieved using 16-ary quadrature amplitude modulation orthogonal frequency division multiplexing and pre-equalization, and an extended distance over 3 m with a data rate of 0.82 Gbps is also presented. The demonstrated high-speed performance shows that micro-LEDs have great potential in the field of UVC communication.

https://doi.org/10.1364/OL.423311

The ultraviolet-C (UVC) spectrum, known as the solar blind region, is located in the 200–280 nm UV spectrum band, in which solar radiation is faint at ground level due to the strong absorption of UV radiation by the ozone layer in the atmosphere [1]. This unique property makes UVC communication have more advantages than traditional visible light communication. First, the low natural background irradiance in the solar blind region can effectively reduce noise interference, which benefits solar blind communication and enables detectors to detect a highly attenuated signal [2]. Second, the strong attenuation of UVC radiation in the atmosphere implies that the radiation power in the non-communication area is minimized and has low detection probability, which ensures an absolutely secure short-range communication [3]. Third, the propagation characteristic of UVC radiation scattered by atmospheric molecules and suspended particles favors realization of the non-line-of-sight communication link [2,4–6]. In particular, indoor links based on UVC radiation can achieve more secure communication because UVC light cannot penetrate ordinary glass or walls [7]. Thus, UVC communication has outstanding performance in terms of security, anti-interference, and diffusion link, is suitable for outdoor solar blind communication, and can also become an interesting alternative for indoor communication to avoid the interference of ambient light and sunlight with high security.

A suitable UVC light source with high optical bandwidth is the basis of a high-speed UVC communication link. Mercury arc lamps were utilized as light sources with limited optical bandwidths in an early study [8]. Recently, the emergence of low-cost and high-output-power LEDs have accelerated the development of UVC communication and its applications in many other fields. UVC LEDs have the advantages of low cost, small size, and low power consumption, making them attractive to realize a high-speed UVC system. Kojima *et al.* demonstrated a 2.08 Gbps communication system over a 1.5 m link based on a 280 nm UVC LED with a −3 dB bandwidth of 153 MHz [9]. Furthermore, they conducted an outdoor experiment to study the performance of a UVC communication system directly exposed to sunlight and achieved a data rate of 1.18 Gbps under a 1.5 m link [10]. Very recently, Alkhazragi *et al.* established a UVC line-of-sight (LOS) link over 1 m with a data rate of 2.4 Gbps utilizing a bit-loading algorithm and discrete multitone (DMT) modulation, and 2 Gbps could still be retained when the link distance was extended to 5 m [11]. The link utilized a 278 nm LED as the transmitter with a −3 dB bandwidth of 170 MHz. Moreover, they further designed a single-input and multiple-output UVC communication link with a reception angle of view of ±9°, and a peak achievable information rate of 1.09 Gbps was realized [12]. All of these remarkable results show that UVC LEDs have great potential application value. However, most researches on UVC communication have been demonstrated by using broad-area UVC LEDs, which have low modulation bandwidths, thus limiting the communication performance. Reducing the LED size is a typical way to increase the modulation bandwidth, because it can simultaneously reduce the carrier lifetime and resistence-capitance time

Table 1. Summary of UVC LED-Based Communication Systems from the Literature and This Work

LED Type	Modulation Scheme	Optical Power	Bandwidth	Data Rate	Distance	Ref.
280 nm LED	PAM-4	3 mW	153 MHz	2.08/1.18 Gbps	1.5 m Indoor/outdoor	[9,10]
278.32 nm LED	DMT	∼6 mW	170 MHz	2.4/2 Gbps	1/5 m	[11]
262 nm micro-LED	OOK/OFDM	∼0.2 mW	438 MHz	0.8/1.1 Gbps	0.3 m	[21]
276.8 nm micro-LED	OFDM	0.854 mW	452.53 MHz	2/1.25/0.82 Gbps	0.5/2.1/3 m	This work

constant [13]. Micro-LEDs have attracted much attention in recent years because they have a low junction temperature and uniform current spreading to obtain a higher current density [14–17]. More importantly, a high current density can effectively reduce the differential carrier lifetime and achieve a higher bandwidth [18]. Moreover, micro-LEDs can be fabricated in the form of series arrays, which can make up for the low output optical power without degrading the modulation bandwidth [19,20]. All these advantages of micro-LEDs are suitable for UVC communication. Therefore, He *et al.* first demonstrated a 1.1 Gbps UVC communication link over 30 cm based on a 262 nm micro-LED with a high bandwidth of 438 MHz, but this initial attempt is not enough to obtain a high data rate and long distance due to the limited optical power [21].

In this Letter, we experimentally achieve high-speed UVC communication based on a 276.8 nm UVC micro-LED. A record −3 dB optical bandwidth of 452.53 MHz at a current density of $500 A/cm^2$ and light output power of 0.854 mW at a current density of $400 A/cm^2$ are obtained with a chip size of 100 μm. The 100 μm micro-LED has a higher optical bandwidth and sufficient optical output power, which can further improve the data rate and transmission distance, as shown in Table 1. Under the condition of meeting the forward error correction (FEC) criterion of 3.8×10^{-3}, a UVC communication link over 0.5 m with a data rate of 2 Gbps is achieved using 16-ary quadrature amplitude modulation orthogonal frequency division multiplexing (16-QAM-OFDM) and pre-equalization. Furthermore, a data rate of 0.82 Gbps in a UVC communication link over 3 m is also presented.

The LED epitaxial wafer was used to fabricate the UVC micro-LED with a size of 100 μm, as shown in Fig. 1(a). The epitaxial layers were grown on a sapphire substrate including mainly a 2 μm thick AlN buffer layer, 1 μm thick unintentional doped AlGaN layer, 1 μm thick n-doped AlGaN layer, 80 nm AlGaN/AlGaN multiple quantum wells, 50 nm thick AlGaN electron blocking layer, 300 nm p-doped AlGaN layer, and 10 nm p-doped contact GaN layer. The device fabrication processes are similar to our previous work [22,23]. A 40 nm ITO layer was deposited on top of the p-GaN to form the current spreading layer. Then standard photolithography, wet etching, and inductively coupled plasma etching were employed to form mesa with the size of 100 μm. Rapid thermal annealing at 550°C was employed to form the ohmic p-contact. A 300 nm SiO_2 layer was deposited as the insulating layer with corresponding holes opening to sputter Ti/Au layers (50 nm/250 nm) as p and n electrodes. The optical microscope image of the 100 μm micro-LED is shown in Fig. 1(b). Figure 1(c) presents the typical current-voltage (I-V) and optical power-current (P-I) curves of a single 100 μm UVC micro-LED. The optical power was measured by attaching the chip to the optical power meter (Thorlabs PM100D), and 0.854 mW at a current density of $400 A/cm^2$ was obtained. The UVC micro-LED has a linear P-I

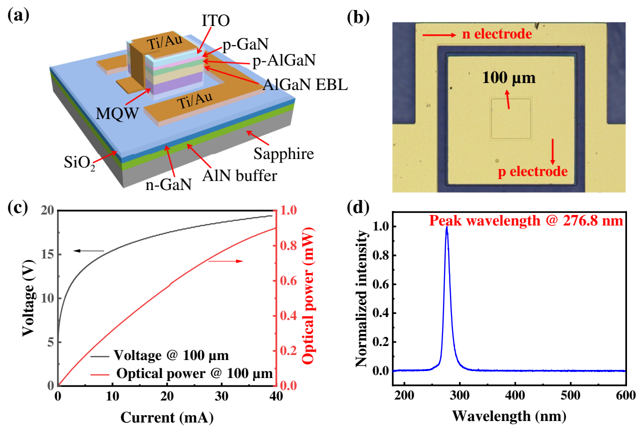

Fig. 1. (a) Schematic diagram of the micro-LED structure. (b) Optical microscope picture of a 100 μm micro-LED. (c) I-V and P-I characteristics of a 100 μm UVC micro-LED. (d) Emission spectrum of a UVC micro-LED at $200 A/cm^2$.

characteristic and high output power, which allows it to have a large dynamic range to accept large amplitude fluctuations of modulated signals, and gives the system a high signal-to-noise ratio (SNR). However, the device has a high operating voltage due to the n- and p-AlGaN layer resistances and the ohmic contact resistance with the metal [24]. Figure 1(d) presents the electroluminescence (EL) spectrum measured by an Ocean Optics USB4000 Spectrometer at $200 A/cm^2$, and the emission peak wavelength is 276.8 nm.

A vector network analyzer (PicoVNA 106) was used to output an AC frequency sweep signal combined with a DC signal through a bias-tee (Mini-circuit ZFBT-6GW) to drive the micro-LED and measure the frequency response. The frequency responses under different driving currents tested by a 1 GHz Si avalanche photodiode (APD, Hamamatsu C5658) are presented in Fig. 2(a). The extracted −3 dB optical modulation bandwidths with a size of 100 μm are 370.69, 412.93, 439.33, 448.24, and 452.53 MHz at currents of 10, 20, 30, 40, and 50 mA, respectively. The increase in bandwidth with the increase in current may be due to the decrease in carrier lifetime at a high current density, which is consistent with the trend of blue micro-LEDs in our previous study [25].

In this work, we used the 100 μm UVC micro-LED described above as the transmitter to build a LOS free-space optical (FSO) communication system, as shown in Fig. 3(a). Considering the received optical power and SNR, the modulation method was chosen as 16-QAM-OFDM. The OFDM data with a symbol length of 2048 and subcarrier number of 512 were first generated by an offline MATLAB program, and the lengths of the cyclic prefix (CP) and pilot sequences were both set as 1/16 of the symbol length. OFDM signals with different bandwidths were tested to obtain the bit error rate (BER) and other

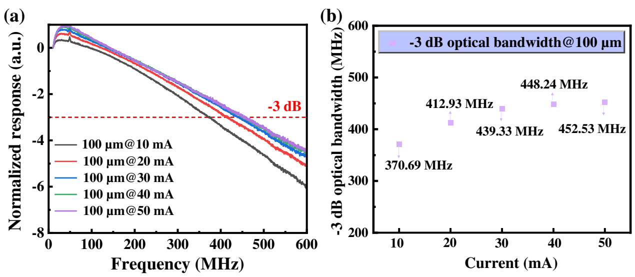

Fig. 2. (a) Frequency responses of a 100 μm UVC micro-LED with different currents. (b) −3 dB optical modulation bandwidth of the UVC micro-LED as a function of current.

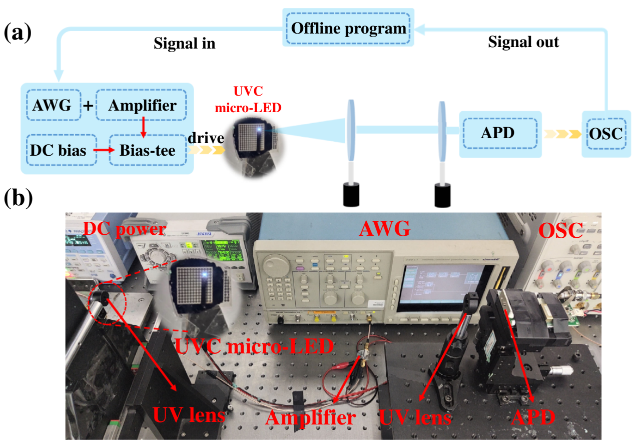

Fig. 3. (a) Experimental setup for FSO communication system based on a UVC micro-LED. (b) Captured photo of the proposed 0.5 m UVC communication system.

parameters by changing the sampling rates of the arbitrary waveform generator (AWG, Tektronix AWG710B, 4.2 Gsa/s). The OFDM data were first uploaded to the AWG, which converted the digital signal into an electrical signal. An amplifier (Mini-circuit ZX60-43-S+) was used to amplify the peak-to-peak voltage of the output electrical signal from AWG. Then the electrical OFDM signal biased by a direct current source (Keithley 2614B) through a bias-tee was used to drive the UVC micro-LED, which was stuck to a quartz glass panel and lit by a high-speed probe. Two lenses with high transmittance to UVC light were simultaneously used to collimate and focus the emitting light into a 100 MHz high-sensitivity APD (Hamamatsu C12702-11) with a response of around 3 A/W to 275 nm, and this APD had a flat frequency response curve to support the expansion of the signal bandwidth. Finally, the received electrical signal was captured by an oscilloscope (OSC, Agilent DSA90604A Infiniium, 20 Gsa/s), which was downloaded to the offline MATLAB program to evaluate the performance. The captured photo of this system is shown in Fig. 3(b).

Based on the 0.5 m UVC system, we first tested the optimum operating condition. Under different drive currents of the UVC micro-LED, the BERs of the 250 MHz 16-QAM-OFDM signal were tested, as shown in Fig. 4(a). The optimum operating current corresponding to the minimum BER was 20 mA. Then fixing the drive current at 20 mA, BERs under different modulation depths were obtained, as shown in Fig. 4(b). The optimum modulation depth was 2.38 V to use the full dynamic range of

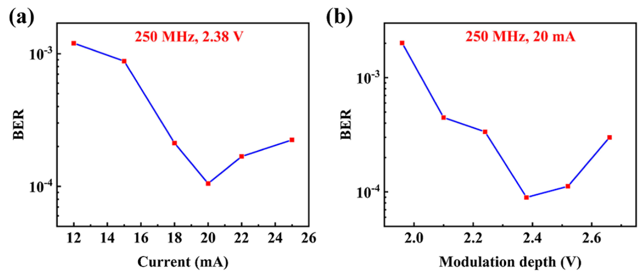

Fig. 4. Fixing bandwidth of OFDM signal at 250 MHz, (a) BER versus drive current and (b) BER versus modulation depth at transmission distance of 0.5 m.

the UVC micro-LED. The following communication tests were all carried out under this optimal operating condition.

First, the performance of BER versus data rate without pre-equalization was obtained, as shown in Fig. 5(a). The BER increases monotonically with the increase in data rate owing to the low response of the system to high frequency signals. With the increase in data rate, the constellation plot becomes scattered owing to the rising number of error symbols. The maximum data rate is 1.36 Gbps over a 0.5 m link with a signal bandwidth around 340 MHz and BER of 3.52×10^{-3} below the FEC threshold. To compensate for the high frequency signal attenuation of the UVC device, a simple one-tap pre-equalization in the frequency domain was used to improve the available signal bandwidth. The pre-equalization was adopted before IFFT and the received signal Y_k can be described as

$$Y_k = \alpha R_k X_k \cdot H_k + N_k, \quad 0 < \alpha < 1, \tag{1}$$

where subscript k represents the index of the subcarriers. X_k is transmitted signal, and H_k is the frequency response of the overall system. R_k is the pre-equalization factor, and is equal to the reciprocal of H_k. N_k is the noise of the overall link, and α is the weighted coefficient adjusted in (0, 1) to obtain the best BER performance. To perform the pre-equalization, we first need to obtain the frequency response of the overall system.

The curve of the BER versus data rate after using pre-equalization is shown in Fig. 5(b). The highest data rate of 2 Gbps was achieved with a BER of 2.86×10^{-3}, and the corresponding power spectra of 500 MHz OFDM signals before and after employing pre-equalization were captured, as shown in the top and bottom of Fig. 5(c), respectively. The attenuation of the spectrum after pre-equalization is relatively gentle. The characteristics of SNR versus bandwidth before and after pre-equalization were also obtained, as shown in Fig. 5(d). The average SNRs were both above 15.8 dB, which was sufficient to support the 16-QAM-OFDM with a certain bandwidth. Without pre-equalization, the curve presents a declining trend, which is consistent with the declined spectrum power. The declined SNR, however, will limit the available bandwidth. An imperfect pre-equalization ($\alpha < 1$) was better due to the non-uniform noise floor, as shown in the inset in Fig. 5(d). With pre-equalization, the SNRs of subcarriers are mostly above 15 dB and become more uniform.

Finally, we extended the transmission distances to 2.1 and 3 m, and their communication performances with pre-equalization are shown in Fig. 6. The optical powers at the receiver side were 25.07, 12.55, and 5.4 μW at distances of 0.5, 2.1, and 3 m, respectively. The highest data rate could still

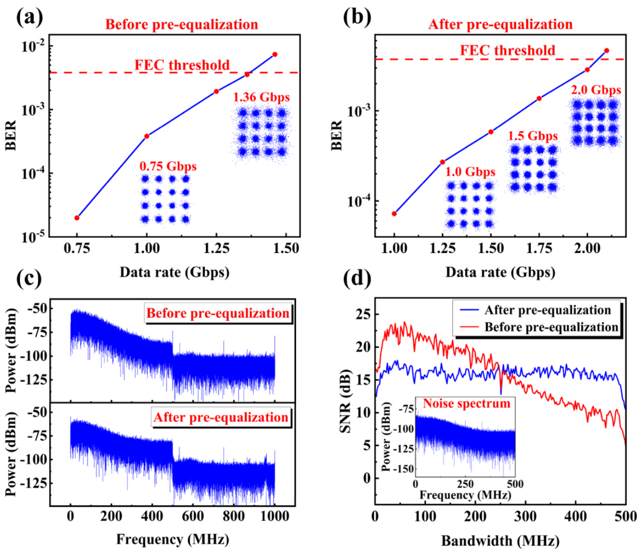

Fig. 5. BER versus data rate at a transmission distance of 0.5 m (a) without pre-equalization and (b) with pre-equalization. Insets are constellation diagrams at different data rates. (c) Power spectra of OFDM signals with bandwidth of 500 MHz before (top) and after (bottom) employing pre-equalization. (d) SNR versus signal bandwidth before and after pre-equalization. Inset is the spectrum of the noise floor.

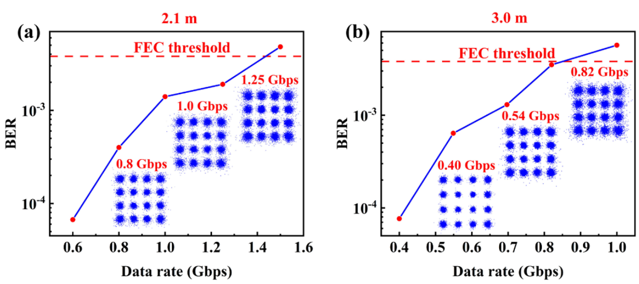

Fig. 6. BER as a function of data rate at a transmission distance of (a) 2.1 m and (b) 3 m. Insets are constellation diagrams of OFDM signal at different data rates.

reach 1.25 Gbps at a distance of 2.1 m. We can obviously find that the performance of the system at 2.1 m is worse than that at 0.5 m mentioned above. The reason is that the atmosphere has a strong attenuation effect on light in the UVC band, which will degrade the received optical power. Similarly, we further extended the transmission distance to 3 m with a highest data rate of 0.82 Gbps, as shown in Fig. 6(b). In the future, we can further improve the data rate by using a higher-bandwidth APD and increasing the output power by a series-connected structure.

In conclusion, a high-speed UVC communication system based on a 276.8 nm UVC micro-LED utilizing 16-QAM-OFDM and pre-equalization was proposed. Modulation bandwidths at various currents were presented and a record −3 dB optical bandwidth of 452.53 MHz was obtained with a chip size of 100 μm at a current density of 500 A/cm^2. This result proves that large-sized UVC micro-LEDs, operating at high optical power, can still have relatively high bandwidths. Moreover, we achieved a UVC link over 0.5 m with a data rate of 2 Gbps and extended the transmission distance to 3 m with a data rate of 0.82 Gbps. These results help build a UVC communication system with better performance in terms of communication speed and distance, but significant enhancement in further distance and faster speed is expected by connecting UVC micro-LEDs in series and optimizing the modulation scheme.

Funding. National Natural Science Foundation of China (61974031); Fudan University-CIOMP Joint Fund (FC2020-001).

Disclosures. The authors declare no conflicts of interest.

Data Availability. Data underlying the results presented in this paper are not publicly available at this time but may be obtained from the authors upon reasonable request.

[†]These authors contributed equally to this work.

REFERENCES

1. Z. Xu and B. M. Sadler, IEEE Commun. Mag. **46**, 67 (2008).
2. R. J. Drost and B. M. Sadler, Semicond. Sci. Technol. **29**, 084006 (2014).
3. M. J. Weisman, F. T. Dagefu, T. J. Moore, C. H. Arslan, and R. J. Drost, Opt. Express **28**, 23640 (2020).
4. S. Arya and Y. H. Chung, IEEE Photon. Technol. Lett. **30**, 895 (2018).
5. S. Arya and Y. H. Chung, J. Opt. Commun. Netw. **11**, 422 (2019).
6. P. Wang and Z. Xu, Opt. Lett. **38**, 2773 (2013).
7. S. Arya and Y. H. Chung, IEEE Syst. J., "Novel indoor ultraviolet wireless communication: design implementation, channel modeling, and challenges," doi:10.1109/JSYST.2020.2995919 (2020).
8. G. Shaw, A. Siegel, and M. Nischan, Proc. SPIE **5071**, 241 (2003).
9. K. Kojima, Y. Yoshida, M. Shiraiwa, Y. Awaji, A. Kanno, N. Yamamoto, and S. Chichibu, in *European Conference on Optical Communication (ECOC)* (2018), pp. 1–3.
10. Y. Yoshida, K. Kojima, M. Shiraiwa, Y. Awaji, A. Kanno, N. Yamamoto, S. F. Chichibu, A. Hirano, and M. Ippommatsu, in *Conference on Lasers and Electro-Optics (CLEO)* (2019), pp. 1–2.
11. O. Alkhazragi, F. Hu, P. Zou, Y. Ha, Y. Mao, T. Ng, N. Chi, and B. S. Ooi, in *Optical Fiber Communication Conference (OFC)* (2020), p. M3I. 5.
12. O. Alkhazragi, F. Hu, P. Zou, Y. Ha, C. H. Kang, Y. Mao, T. K. Ng, N. Chi, and B. S. Ooi, Opt. Express **28**, 9111 (2010).
13. K. J. Singh, Y.-M. Huang, T. Ahmed, A.-C. Liu, S.-W. H. Chen, F.-J. Liou, C.-C. L. T. Wu, C.-W. Chow, G.-R. Lin, and H.-C. Kuo, Appl. Sci. **10**, 7384 (2020).
14. P. Tian, J. J. D. McKendry, Z. Gong, B. Guilhabert, I. M. Watson, E. Gu, Z. Chen, G. Zhang, and M. D. Dawson, Appl. Phys. Lett. **101**, 231110 (2012).
15. Z. Gong, S. Jin, Y. Chen, J. McKendry, D. Massoubre, I. M. Watson, E. Gu, and M. D. Dawson, J. Appl. Phys. **107**, 013103 (2010).
16. X. Zhou, P. Tian, C.-W. Sher, J. Wu, H. Liu, R. Liu, and H.-C. Kuo, Prog. Quantum Electron. **71**, 100263 (2020).
17. S. Zhu, X. Chen, X. Liu, G. Zhang, and P. Tian, Prog. Quantum Electron. **73**, 100274 (2020).
18. R. P. Green, J. J. D. McKendry, D. Massoubre, E. Gu, M. D. Dawson, and A. E. Kelly, Appl. Phys. Lett. **102**, 091103 (2013).
19. A. D. Griffiths, J. Herrnsdorf, J. J. D. McKendry, M. J. Strain, and M. D. Dawson, Philos. Trans. Roy. Soc. A **378**, 20190185 (2020).
20. E. Xie, R. Bian, X. He, M. S. Islim, C. Chen, J. J. D. McKendry, E. Gu, H. Haas, and M. D. Dawson, IEEE Photon. Technol. Lett. **32**, 499 (2020).
21. X. He, E. Xie, M. S. Islim, A. A. Purwita, J. J. D. McKendry, E. Gu, H. Haas, and M. D. Dawson, Photon. Res. **7**, B41 (2019).
22. X. Liu, R. Lin, H. Chen, S. Zhang, Z. Qian, G. Zhou, X. Chen, X. Zhou, L. Zheng, R. Liu, and P. Tian, ACS Photon. **6**, 3186 (2019).
23. P. Tian, X. Liu, S. Yi, Y. Huang, S. Zhang, X. Zhou, L. Hu, L. Zheng, and R. Liu, Opt. Express **25**, 1193 (2017).
24. M. Kneissl and J. Rass, *III-Nitride Ultraviolet Emitters* (Springer, 2016).
25. S. Mei, X. Liu, W. Zhang, R. Liu, L. Zheng, R. Guo, and P. Tian, ACS Appl. Mater. Interfaces **10**, 5641 (2018).